Symmetry Strategy for Rapid Discovery of Abundant Fractional Quantum Ferroelectrics

Guoliang Yu,[1,*] Junyi Ji,[1,2,*] Yingwei Chen,[1] Changsong Xu,[1,†] and H. J. Xiang[1,‡]
[1]Key Laboratory of Computational Physical Sciences (Ministry of Education), Institute of Computational Physical Sciences, State Key Laboratory of Surface Physics, and Department of Physics, Fudan University, Shanghai 200433, China
[2]Beijing National Laboratory for Condensed Matter Physics and Institute of Physics, Chinese Academy of Sciences, Beijing 100190, China

(Received 28 April 2024; accepted 4 December 2024; published 8 January 2025)

Traditional ferroelectrics are limited by Neumann's principle, which confines exploration of ferroelectrics within polar point groups. Our recent work [Ji *et al.*, Nat. Commun. **15**, 135 (2024)] proposes the concept of fractional quantum ferroelectricity (FQFE) that extends the playground of ferroelectricity to nonpolar point groups. Here, we apply group theory and introduce an efficient symmetry strategy to identify FQFE candidates. Integrated with a high-throughput screening scheme, we go through 171 527 materials and identify 221 potential FQFE candidates, which are already experimentally synthesized. In addition, we point out for the first time that the essence of FQFE is fractional atomic displacements with respect to lattice vectors, which can actually result in both fractional (type I) and integer (type II) quantized polarization, respectively. Through performing first-principles calculations, we verify the symmetry-predicted switchable FQFE properties in bulk $AlAgS_2$ and monolayer HgI_2. Notably, $AlAgS_2$ exhibits an ultralow switching barrier of 22 meV/f.u. and interlocked in-plane/out-of-plane polarization, while HgI_2 displays large spontaneous polarization of 42 $\mu C/cm^2$. Our findings not only advance the understanding on FQFE, but also offer guidance for experimental exploration and design of novel ferroelectric materials.

DOI: 10.1103/PhysRevLett.134.016801

Introduction—Ferroelectric (FE) material is essential for various applications in energy-efficient nanoelectronic devices and storage [1–5]. For conventional FEs, the polarization arises from small atomic displacements [see Fig. 1(a)], which corresponds to the variants in Wyckoff positions, such as the z component of $(0.5, 0.5, z)$. In such cases, the direction of polarization must be consistent with the symmetry of the FE phase, as required by Neumann's principle [6], which limits the exploration of ferroelectricity to the 10 polar point groups out of the total 32 ones [7–10].

Recently, we proposed a new concept of fractional quantum ferroelectricity (FQFE) [11], characterized by unconventional polarization arising from fractional atomic displacements with respect to lattice vectors [see Figs. 1(b) and 1(c)]. Unlike conventional ferroelectrics, FQFE violates Neumann's principle. In FQFE systems, displacements occur for ion(s) from high-symmetry points or lines to another equivalent position, maintaining the energy and symmetry of both the initial and final states. For example, in monolayer α-In_2Se_3, the in-plane position of the Se ion moves from the Wyckoff position $(1/3, 2/3)$ to $(2/3, 1/3)$, leading to an unexpected in-plane polarization [12–15]. A key aspect in FQFE is the polarization quantum, which refers to the polarization induced by a unit charge e passing through the distance of a lattice vector $\boldsymbol{a}$, defined as $\mathbf{Q} = (e/\Omega)\boldsymbol{a}$ (Ω denotes the volume of the cell) [16,17]. The FQFE can exist in 27 different point groups, including 7 polar and 20 nonpolar ones, significantly expanding the pool of ferroelectrics. FQFE materials exhibit large atomic displacements, resulting in substantial spontaneous polarization, making them appealing in fundamental physics and advanced applications.

Despite the wide theoretical existence of FQFEs, currently known FQFE systems are limited to monolayer α-In_2Se_3 and bulk zinc-blende AgBr. Moreover, though AgBr is perfect for theoretical demonstration of FQFE in a nonpolar point group, it is experimentally found unstable in air. The scarcity of FQFE candidates leads to challenges to experimental exploration of the intriguing physics and promising application of FQFE. The scarcity of FQFEs can be attributed to their adherence to symmetry rules that are distinct from common understanding, potentially resulting in the overlooking of possible FQFEs [7–10]. A practical problem is that, if certain structure is assumed to be one state of FQFE, there still lacks an effective method to determine the other different but symmetrically equivalent state (or other states). It is thus highly desirable to develop an efficient method to rapidly identify possible FQFEs.

In this Letter, we develop an efficient symmetry strategy for rapid discovery of FQFEs. Such strategy utilizes group

*These authors contributed equally to this work.
†Contact author: csxu@fudan.edu.cn
‡Contact author: hxiang@fudan.edu.cn

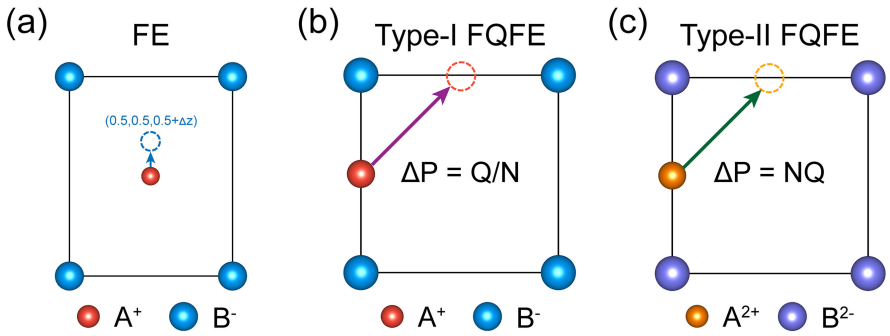

FIG. 1. Classification of ferroelectrics. Schematics of (a) conventional FE, (b) type-I FQFE, and (c) type-II FQFE. The type-I and type-II FQFE systems exhibit ferroelectricity with fractional and integer quantized polarizations, respectively. The arrows indicate the direction of movements, while dashed circles represent the destination of movements. The valence states of the ions are given at the bottom of the figure.

theory analysis and involves lattice symmetry. Applying such a strategy, a high-throughput first-principles screening workflow is performed to search potential FQFE candidates. Running through over 171 000 materials, we identify 221 experimentally synthesized materials as FQFE candidates, with 21 candidates in polar point groups and 200 in nonpolar ones. Based on the screening results, the FQFEs are newly classified into type I and type II, where the latter actually exhibits integer quantized polarization. Moreover, through further density functional theory (DFT) calculations, bulk $AlAgS_2$ is found to exhibit interlocked in-plane type-I FQFE and out-of-plane conventional ferroelectricity, with an ultralow switching barrier of 22 meV/f.u. More interestingly, type-II FQFE is demonstrated in monolayer HgI_2 with a nonpolar point group and it exhibits a large polarization of 42 $\mu C/cm^2$.

Classification of the FQFE—According to the FQFE theory, the atomic displacements should be fractional lattice vectors and the polarization should intuitively be fractional multiples of polarization quantum [11]. Such a simple case is termed as type-I FQFE here. As exampled by the tetragonal system in Fig. 1(a), it is assumed that the sites $(0, 1/2, 0)$ and $(1/2, 1, 0)$ are equivalent. When the A^+ ion moves $1/2$ of the lattice along the [110] direction from position $(0, 1/2, 0)$ to $(1/2, 1, 0)$, it induces a polarization difference $\Delta\mathbf{P} = \mathbf{Q}/2$. However, a different case is that, though displacements are fractional, the polarization is integer times of polarization quantum, which case is termed as type-II FQFE. For instance, as shown in Fig. 1(b), A^{2+} ion displaces in the same way with that in Fig. 1(a), while the polarization difference yields $\Delta\mathbf{P} = \mathbf{Q}$. Another scenario leading to type-II FQFE is that, though the charge of A is $+1$, the multiplicity of A ions in its conventional cell is an even number. Note that both types of FQFE correspond to atomic displacements that are fractional multiples of lattice vectors.

Symmetry strategy and high-throughput screening of FQFE—Applying group theory analysis, we develop a symmetry strategy to identify FQFE, as illustrated in Fig. 2(a). Specifically, the identification process follows four steps. (i) Given a crystal structure of FE phase L_1, find its space group G_L, and the space group G_{latt} of its symmetrized lattice. (ii) Construct all other FE phase structure L_2 in the way that $L_2 = hL_1$, where h is a symmetry operation in G_{latt}/G_L (i.e., belonging to G_{latt} but not to G_L). (iii) For each L_2, check whether the phase transition from L_1 to L_2 is likely to be FQFE. This can be determined by whether $\Delta d_{A,\alpha}(\alpha = x, y, z)$, the total displacement of the element A along the α direction, is a fraction M/N. Here, $\Delta d_{A,\alpha} = \Sigma_i d^i_{L2,A,\alpha} - d^i_{L1,A,\alpha} = M/N(\alpha = x, y, z, N = 2, 3, 4, 6, 8; M = 1, 2, \ldots, N-1)$, where $d^i_{L1,A,\alpha}$ and $d^i_{L2,A,\alpha}$ represent the α fractional coordinates of the ith A atom in the L_1 and L_2 phases, respectively. Note that this step should be performed in both primitive cell and conventional cell, as type-II FQFE can possibly be overlooked if only examining $\Delta d_{A,\alpha}$ in the primitive cell (see Sec. 2 in the Supplemental Material (SM) [18]), e.g., $CuCrS_2$ shown in Fig. S2(g). (iv) Output the fraction $\Delta d_{A,\alpha}$ and corresponding L_2. To better understand this strategy, we use CuCl as an example [Fig. 2(b)]. (i) The space group of the L_1 phase CuCl is $G_L = F\text{-}43m$. Removing all atoms, the lattice space group is found to be $G_{\text{latt}} = Fm\text{-}3m$. (ii) h is a symmetry operation belonging to $Fm\text{-}3m$ but not to $F\text{-}43m$. Take $h = I$ (inversion) as an example, another FE phase L_2 can be constructed as $L_2 = IL_1$. Note that other choices of h will lead to the same FE phase L_2 (see Sec. 3 in SM [18]). (iii) In the unit cells of L_1 and L_2, the Cu atom at (0,0,0) is invariant under I, while the Cl atom moves from $(1/4, 1/4, 1/4)$ to $(3/4, 3/4, 3/4)$. Hence, $\Delta d_{\text{Cu},\alpha} = 0$ and $\Delta d_{\text{Cl},\alpha} = (1/2, 1/2, 1/2)$, making CuCl a candidate for FQFE (see Fig. 1 and Supplemental Material, Table S1 [18]).

To extensively identify FQFEs, besides the presently developed symmetry strategy, the high-throughput screening combined with DFT is also necessary [37–41]. As shown in Fig. 2(c), our search starts with over 171 000 experimentally synthesized materials from the Materials Project [19] and Computational 2D Materials Database (C2DB) [20,21]. Subsequently, we exclude materials with

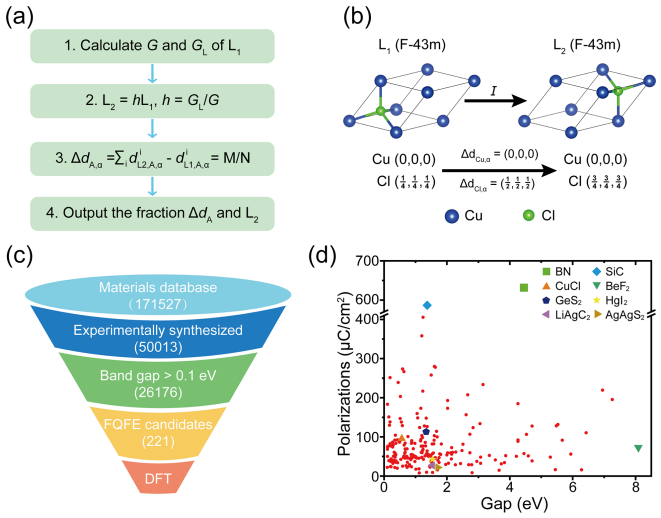

FIG. 2. Symmetry strategy and high throughput screenings of the FQFE candidates. (a) The identification of FQFE candidates. G is the space group of L_1 phase, while and G_L is that of its lattice. $\Delta d_{A,\alpha}(\alpha = x, y, z)$ is the total displacement of the A atom (s) along the α direction in the phase transition from L_1-L_2, while $d^i_{L1,A,\alpha}$ and $d^i_{L2,A,\alpha}$ represent the α coordinates of the i th A atom in the L_1 and L_2 phases. Note that N and M choose their values from $N = 2, 3, 4, 6, 8$, $M = 1, 2, \ldots, N-1$. (b) FQFE in bulk CuCl with space group of the F-43m. (c) The high-throughput screening workflow of FQFE. (d) Spontaneous polarization versus band gap for FQFE candidates. The values of band gaps are extracted from the Materials Project [19] and C2DB [20,21].

band gaps smaller than 0.1 eV due to potential leakage, leaving 26 176 materials. Then, we apply the presently developed symmetry strategy, which has been integrated in the PASP software [22]. Finally, 221 FQFE candidates, with 21 in polar groups and 200 in nonpolar groups, was further verified through DFT calculations. Such 221 candidates are further classified into 27 crystal types (see Table I, Fig. S2, Tables S1 and S2 [18]). For example, zinc-blende structure with chemical formula AB (F-43m) belongs to the CuCl type. Among these candidates, monolayer α-In_2Se_3 [13,14], bulk $CuCrS_2$ [42], $CuCrSe_2$ [43,44], and $AgCrS_2$ [45] have been experimentally confirmed to exhibit in-plane polarization, validating the FQFE theory and the present symmetry strategy.

TABLE I. Classification of FQFE candidates. The numbers in parentheses indicate the number of materials of that type. The "other" type contains eight types and nine compounds.

Space group	Structural type	Space group	Structural type
F-43m	CuCl type (27)	P-6m2	$LiAuC_2$ type (2)
	DyNiBi type (42)		GaSe type (4)
I-4	$GaCuI_4$ type (7)		MoS_2-type (12)
	Hg_2GeSe_4 type (32)		BaLiAs-type (7)
P-42c	$AlCuCl_4$ type (4)	P-6c2	$BaTi(SiO_3)_3$-type (6)
$P3m1$	$AlAgS_2$ type (3)	$P63/m$	B_2Cl_6-type (3)
	SrAlSiH type (6)	P-3m1	CaI_2-type (35)
$R3m$	$CuCrS_2$ type (4)	P-4m2	HgI_2-type (4)
	WS_2 type (5)	$P6_222$	SiO_2-type (2)
$P312$	$KNiIO_6$ type (7)	Other	8 types (9)

Let us take an overview of the obtained FQFE candidates. In Fig. 2(d), we present a summary of the band gap versus polarization for all FQFE candidates. As aforementioned, FQFEs generally exhibit significant spontaneous polarization due to their substantial atomic displacements. For instance, monolayers of HgI_2 and GeS_2 with the P-4m2 space group display polarizations of 42.0 and 113.2 μC/cm^2, respectively, while the bulk BN, SiC, and CuCl with the F-43m space group demonstrate even higher values, reaching 631.7, 586.6, and 96.7 μC/cm^2, respectively. Among these materials, bulk BeF_2 with a space group of $P6_222$ exhibits the largest band gap of 8.09 eV, accompanied by a spontaneous polarization of 71.4 μC/cm^2. We further examine the polarization switching barrier but did not calculate it for all candidates, as pathway predicted by the climbing image nudged elastic band (CI-NEB) method [23] may not reflect the real switching process. Instead, we selectively choose ionic systems with simple crystal structure, which generally have lower switching barriers and are well suited to the CI-NEB method (see Table S3). In the following sections, we demonstrate FQFE of bulk $AlAgS_2$ and monolayer HgI_2, which both exhibit low polarization switch barriers.

Type-I FQFE in bulk $AlAgS_2$—The bulk $AlAgS_2$ has been experimentally synthesized [46] and its structure can be viewed as two AlS_2 layers intervened by a layer of Ag ions [see Fig. 3(a)]. The $AlAgS_2$ displays a band gap of 1.71 eV, and the Ag ion exhibit +1 valence state. First, we applied the symmetry strategy to identify the FQFE of $AlAgS_2$. As shown in Fig. 3(a), the space group of the L_1 phase $AlAgS_2$ is $G_L = P3m1$, while the space group of its lattice is $G_{\text{latt}} = P$-3m1. Another phase, L_2, equivalent to L_1, can be constructed by $L_2 = hL_1$, where $h = G_{\text{latt}}/G_L$ represents a symmetry operation. Presently, h can choose from inversion symmetry I centered at any Al atom, and twofold rotation C_2 along the line connecting any Al atom and its nearest Al neighbor, both of which can lead to the same L_2 phase. As illustrated in Fig. 3(a), under the symmetry operation h, the positions of Al and S atoms remain invariant in the L_1 and L_2 phases, while those of Ag atoms change from $(2/3, 2/3, z)$ to $(1/3, 1/3, -z)$. As a result, the displacement of the Al, S, and Ag atoms are $\Delta d_{\text{Al},\alpha} = 0$, $\Delta d_{\text{S},\alpha} = 0$, and $\Delta d_{\text{Ag},\alpha} = (1/3, 1/3, 2z)$, respectively. Therefore, $AlAgS_2$ emerges as a potential candidate for FQFE owing to the fractional in-plane displacement of $\frac{1}{3}\mathbf{a} + \frac{1}{3}\mathbf{b}$ of the Ag ions.

Further, we validated the in-plane polarization arising from FQFE in bulk $AlAgS_2$ by DFT calculations. Figure 3(b) shows the evolution of the in-plane polarizations along the L_1-TS-L_2 pathway (TS stands for transition state) calculated

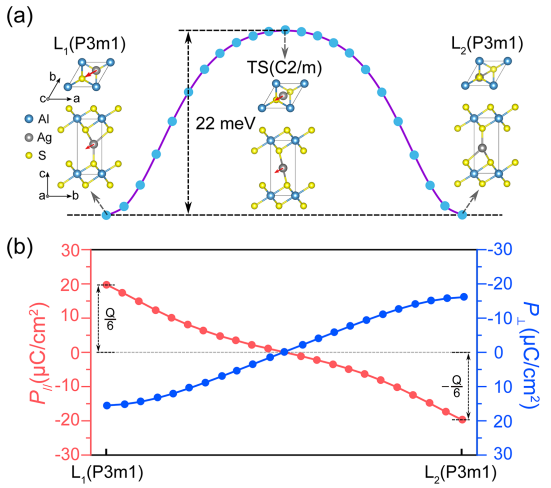

FIG. 3. Type-I FQFE in bulk $AlAgS_2$. (a) Geometric structures and polarization switching barrier of $AlAgS_2$. The $L_{1/2}$ phase belongs to $P3m1$ and the TS belongs to $C2/m$. The red arrow denotes the displacement of central Ag atoms, including an in-plane component of $\frac{1}{3}\mathbf{a}+\frac{1}{3}\mathbf{b}$ and a small out-of-plane displacement. (b) The evolution of in-plane and out-of-plane along the L_1-TS-L_2 pathway. The in-plane polarization $\mathbf{P}_{||}$ of the $L_{1/2}$ phases are $\pm 21.97\ \mu C/cm^2$ along the [110] direction. $\mathbf{Q}=131.82\ \mu C/cm^2$ is the polarization quantum along the [110] direction. Thus, the $\mathbf{P}_{||}=\pm\mathbf{Q}/6$ and the polarization difference between L_1 and L_2 phases is $\Delta\mathbf{P}=\mathbf{Q}/3$. The out-of-plane polarization $\mathbf{P}_{\perp}$ of the $L_{1/2}$ phases determined to be $\pm 15.55\ \mu C/cm^2$.

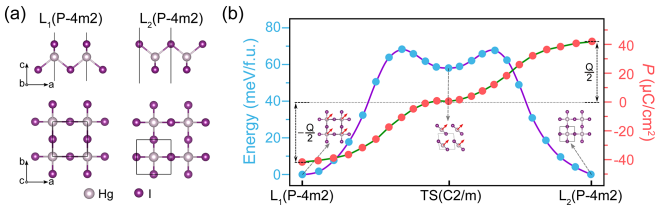

FIG. 4. Type-II FQFE in monolayer HgI_2. (a) Geometric structure of HgI_2 for the L_1 and L_2 phases. (b) The energy barrier and the evolution of the polarization along the L_1-TS-L_2 pathways. The red arrows denote that the Hg atoms displace along the [110] direction. Here, the polarizations of $L_{1/2}$ phases are $\mathbf{P}_{1/2}=\pm\mathbf{Q}/2=\pm 42.0\ \mu C/cm^2$. Thus, the polarization difference is $\Delta\mathbf{P}=\mathbf{Q}$, which is an integer multiple of the polarization quantum. $\mathbf{Q}$ is the polarization quantum along the [110] direction.

by the Berry phase method [24–26]. One can see that the L_1 and L_2 phases have in-plane polarizations with amplitudes 21.97 and $-21.97\ \mu C/cm^2$, respectively. The polarization quantum Q of $AlAgS_2$ along the [110] direction is $131.82\ \mu C/cm^2$, which is obtained by $\mathbf{Q}=(e/\Omega)\mathbf{a}$, where e, $\mathbf{a}$, and Ω represent the electron charge, lattice vector along the [110] direction, and the volume of the unit cell. Therefore, the in-plane polarization of $AlAgS_2$ is type-I FQFE, and the polarization difference between the L_1 and the L_2 phase is $\Delta\mathbf{P}=\mathbf{Q}/3$. Furthermore, to further demonstrate the ferroelectricity of $AlAgS_2$, we show that the polarization can be readily switched by the application of an external electric field. Figure 3(a) also shows the minimum energy pathway of two low-symmetry phase L_1 and L_2 using the CI-NEB method [23]. One can see that the transforming between L_1 and L_2 phases only needs to overcome an energy barrier of about 22 meV/f.u., which is much smaller than the 200 meV/f.u. in the experimentally confirmed FE $PbTiO_3$ [47]. *Ab initio* molecular dynamics shows that an ultralow electric field of $E_{110}=0.025\ V/Å$ is sufficient to overcome such a small barrier (see Sec. 6 in SM [18]). This ultralow polarization switched electric field indicating that the FQFE of $AlAgS_2$ is likely to be experimentally confirmed. Therefore, these results determine that bulk $AlAgS_2$ has switchable in-plane type-I FQFE.

In addition, as shown in Fig. 3(a), a difference exists in the distance between the central Ag atomic layer and the two S atomic layers in $AlAgS_2$, leading to inversion symmetry breaking and inducing conventional out-of-plane ferroelectricity. The out-of-plane dipole moment of $AlAgS_2$ is $15.55\ \mu C/cm^2$ [see Fig. 3(b)]. Interestingly, the out-of-plane and in-plane polarization are interlocked, akin to the 2D room temperature FE α-In_2Se_3 [12–14]. It is noteworthy that there exists a series of materials isostructural with $AlAgS_2$ that exhibit similar switchable ferroelectricity, such as the experimentally synthesized bulk $LuCuS_2$ and $ScCuCS_2$ [48,49] (see Sec. 7 in SM [18]). Moreover, type-I FQFE can exist not only in materials with polar point groups like $AlAgS_2$ but also in materials with nonpolar point groups, such as $LiAC_2$ (A = Ag and Au) with D_{3h} point group (see Sec. 8 in SM [18]).

Type-II FQFE in monolayer HgI_2—We now investigate the monolayer HgI_2 that survives in the FQFE screening. Bulk HgI_2, a van der Waals layered material, has been experimentally synthesized [50,51]. The cleavage energy of monolayer HgI_2 is $0.21\ J/m^2$ (see Fig. S5 [18]), significantly lower than successfully exfoliated materials like graphene ($0.46\ J/m^2$) [52] and MoS_2($0.42\ J/m^2$) [53], suggesting it can be readily obtained through mechanical exfoliation. Monolayer HgI_2 has a tetragonal lattice (P-4m2 space group, nonpolar D_{2d} point group), as shown in Fig. 4(a). The L_2 phase can be constructed from L_1 by symmetry operations h, where h can be inversion symmetry I, gliding mirror symmetry, fourfold rotation, twofold screw, or mirror symmetry. Based on our symmetry strategy analysis, the HgI_2 monolayer is a candidate for FQFE because the fractional displacement of the Hg atoms is $\Delta d_{\mathrm{Hg},\alpha}=(1/2,1/2,0)$ [see Fig. 4(a)]. However, due to the +2 valence state of the Hg ion, the system yields an integer polarization difference of $\Delta\mathbf{P}=\mathbf{Q}$ along the [110] direction, which demonstrates HgI_2 as a type-II FQFE.

We further demonstrated the FQFE nature of HgI_2 by DFT calculations. First, we verify the thermal and dynamic

stability by performing phonon and molecular dynamics simulations at 300 K for the low-symmetry phase. The absence of imaginary frequencies of phonons and the structural integrity after 5 ps confirm the stability and robustness at room temperature (Fig. S6 in SM [18]). Then, we calculated the switching barrier from L_1 to L_2, which is 68 meV/f.u. [Fig. 4(b)], significantly lower than traditional bulk FE materials like $PbTiO_3$ (200 meV/f.u.) [47]. This lower barrier likely arises from the Hg^{2+} ion's d^{10} configuration, facilitating ion diffusion [54], similar to Ag^+ in $AgCrS_2$ [55] and the Cu^+ in $CuInP_2S_6$ [56]. The spontaneous polarization of the monolayer HgI_2 was determined using the Berry phase method [24–26]. With an effective thickness of 6 Å, the polarizations of the L_1 and L_2 phases along [110] are -42.0 and 42.0 $\mu C/cm^2$, respectively. The polarization quantum is 84.0 $\mu C/cm^2$, according to the definition of $\mathbf{Q} = (e/\Omega)\mathbf{a}$ in modern polarization theory. The polarization difference between L_1 and L_2 is $\Delta\mathbf{P} = \mathbf{Q}$, thus verifying that the monolayer HgI_2 is a type-II FQFE with an integer quantized polarization. These above results confirm that monolayer HgI_2 with nonpolar point group possesses spontaneous and switchable type-II FQFE.

In summary, we develop a new method for identifying FQFE based on new symmetry principles. By integrating this method with high-throughput screening, we pinpoint 221 FQFE candidates, including 21 candidates within polar groups and 200 within nonpolar groups. Through application of the FQFE theory and DFT calculations, we further validated the FQFE properties in $AlAgS_2$ and HgI_2 systems. Notably, we find that the $AlAgS_2$ exhibits an ultralow switching barrier and its in-plane (FQFE) and out-of-plane (conventional FE) spontaneous polarizations measure 21.97 and 15.55 $\mu C/cm^2$, respectively. Additionally, monolayer HgI_2 exhibits large spontaneous polarization with 42 $\mu C/cm^2$. Our findings not only advance the understanding of FQFE but also provide various FQFE candidates for experimental verification.

Acknowledgments—We acknowledge financial support from the National Key R&D Program of China (No. 2022YFA1402901), NSFC (12188101, 12174060, and 12274082), the Guangdong Major Project of the Basic and Applied Basic Research (Future functional materials under extreme conditions—2021B0301030005), Shanghai Science and Technology Program (No. 23JC1400900), and Shanghai Pilot Program for Basic Research—FuDan University 21TQ1400100 (23TQ017). C. X. also acknowledges support from the Innovation Program for Quantum Science and Technology (ZD0220240201), the Shanghai Science and Technology Committee (Grant No. 23ZR1406600) and the Xiaomi Young Talents Program. J. J. also acknowledges the support from China National Postdoctoral Program for Innovative Talents (BX20230408).

[1] V. Garcia and M. Bibes, Ferroelectric tunnel junctions for information storage and processing, Nat. Commun. **5**, 4289 (2014).
[2] L. W. Martin and A. M. Rappe, Thin-film ferroelectric materials and their applications, Nat. Rev. Mater. **2**, 16087 (2016).
[3] J. P. Velev, J. D. Burton, M. Y. Zhuravlev, and E. Y. Tsymbal, Predictive modelling of ferroelectric tunnel junctions, npj Comput. Mater. **2**, 16009 (2016).
[4] P. Shivashankar and S. Gopalakrishnan, Review on the use of piezoelectric materials for active vibration, noise, and flow control, Smart Mater. Struct. **29**, 053001 (2020).
[5] L. Qi, S. Ruan, and Y. J. Zeng, Review on recent developments in 2D ferroelectrics: Theories and applications, Adv. Mater. **33**, e2005098 (2021).
[6] F. L. Neumann and O. E. Meyer, *Vorlesungen über Die Theorie Der Elasticität Der Festen Körper Und Des Lichtäthers: Gehalten an Der Universität Königsberg* (B. G. Teubner-Verlag, Leipzig, 1885).
[7] D. Litvin, Ferroelectric space groups, Acta Cryst allogr. **42**, 44 (1986).
[8] H. Schmid, Some symmetry aspects of ferroics and single phase multiferroics, J. Phys. Condens. Matter **20**, 434201 (2008).
[9] P. P. Shi, Y. Y. Tang, P. F. Li, W. Q. Liao, Z. X. Wang, Q. Ye, and R. G. Xiong, Symmetry breaking in molecular ferroelectrics, Chem. Soc. Rev. **45**, 3811 (2016).
[10] P. F. Li, W. Q. Liao, Y. Y. Tang, W. Qiao, D. Zhao, Y. Ai, Y. F. Yao, and R. G. Xiong, Organic enantiomeric high-T_c ferroelectrics, Proc. Natl. Acad. Sci. U.S.A. **116**, 5878 (2019).
[11] J. Ji, G. Yu, C. Xu, and H. J. Xiang, Fractional quantum ferroelectricity, Nat. Commun. **15**, 135 (2024).
[12] W. Ding, J. Zhu, Z. Wang, Y. Gao, D. Xiao, Y. Gu, Z. Zhang, and W. Zhu, Prediction of intrinsic two-dimensional ferroelectrics in In_2Se_3 and other III_2-IV_3 van der Waals materials, Nat. Commun. **8**, 14956 (2017).
[13] C. Cui, W. J. Hu, X. Yan, C. Addiego, W. Gao, Y. Wang, Z. Wang, L. Li, Y. Cheng, P. Li *et al.*, Intercorrelated in-plane and out-of-plane ferroelectricity in ultrathin two-dimensional layered semiconductor In_2Se_3, Nano Lett. **18**, 1253 (2018).
[14] J. Xiao, H. Zhu, Y. Wang, W. Feng, Y. Hu, A. Dasgupta, Y. Han, Y. Wang, D. A. Muller, L. W. Martin *et al.*, Intrinsic two-dimensional ferroelectricity with dipole locking, Phys. Rev. Lett. **120**, 227601 (2018).
[15] L. Wang, X. Wang, Y. Zhang, R. Li, T. Ma, K. Leng, Z. Chen, I. Abdelwahab, and K. P. Loh, Exploring ferroelectric switching in α-In_2Se_3 for neuromorphic computing, Adv. Funct. Mater. **30**, 2004609 (2020).
[16] R. Resta and D. Vanderbilt, in *Physics of Ferroelectrics: A Modern Perspective* (Springer, New York, 2007), p. 31.
[17] N. A. Spaldin, A beginner's guide to the modern theory of polarization, J. Solid State Chem. **195**, 2 (2012).
[18] See Supplemental Material at http://link.aps.org/supplemental/10.1103/PhysRevLett.134.016801 for computational details, FQFE in primitive and conventional cells, construct L_2 phase, FQFE candidate materials by high-throughput search, barriers for the FQFE candidate materials, AIMD simulations under the electric field, type-I FQFE in bulk $AlAgS_2$ type with polar point groups and bulk $LiAC_2$

with nonpolar point groups, cleavage energies and stability of monolayer HgI_2, and polarization switching in periodic and finite FQFE system, which includes Refs. [19–36].

[19] A. Jain, S. P. Ong, G. Hautier, W. Chen, W. D. Richards, S. Dacek, S. Cholia, D. Gunter, D. Skinner, G. Ceder *et al.*, Commentary: The materials project: A materials genome approach to accelerating materials innovation, APL Mater. **1**, 011002 (2013).

[20] S. Haastrup, M. Strange, M. Pandey, T. Deilmann, P. S. Schmidt, N. F. Hinsche, M. N. Gjerding, D. Torelli, P. M. Larsen, A. C. Riis-Jensen *et al.*, The computational 2D materials database: High-throughput modeling and discovery of atomically thin crystals, 2D Mater. **5**, 042002 (2018).

[21] M. N. Gjerding, A. Taghizadeh, A. Rasmussen, S. Ali, F. Bertoldo, T. Deilmann, N. R. Knøsgaard, M. Kruse, A. H. Larsen, S. Manti *et al.*, Recent progress of the computational 2D materials database (C2DB), 2D Mater. **8**, 044002 (2021).

[22] F. Lou, X. Y. Li, J. Y. Ji, H. Y. Yu, J. S. Feng, X. G. Gong, and H. J. Xiang, PASP: Property analysis and simulation package for materials, J. Chem. Phys. **154**, 114103 (2021).

[23] G. Henkelman, B. P. Uberuaga, and H. Jónsson, A climbing image nudged elastic band method for finding saddle points and minimum energy paths, J. Chem. Phys. **113**, 9901 (2000).

[24] R. Resta, Theory of the electric polarization in crystals, Ferroelectrics **136**, 51 (1992).

[25] R. D. King-Smith and D. Vanderbilt, Theory of polarization of crystalline solids, Phys. Rev. B **47**, 1651 (1993).

[26] R. Resta, Macroscopic polarization in crystalline dielectrics: The geometric phase approach, Rev. Mod. Phys. **66**, 899 (1994).

[27] G. Kresse and J. Furthmüller, Efficient iterative schemes for *ab initio* total-energy calculations using a plane-wave basis set, Phys. Rev. B **54**, 11169 (1996).

[28] J. P. Perdew, K. Burke, and M. Ernzerhof, Generalized gradient approximation made simple, Phys. Rev. Lett. **77**, 3865 (1996).

[29] P. E. Blöchl, Projector augmented-wave method, Phys. Rev. B **50**, 17953 (1994).

[30] G. Kresse and D. Joubert, From ultrasoft pseudopotentials to the projector augmented-wave method, Phys. Rev. B **59**, 1758 (1999).

[31] A. Togo and I. Tanaka, First principles phonon calculations in materials science, Scr. Mater. **108**, 1 (2015).

[32] L. Chen, C. Xu, H. Tian, H. Xiang, J. Íñiguez, Y. Yang, and L. Bellaiche, Electric-field control of magnetization, Jahn-Teller distortion, and orbital ordering in ferroelectric ferromagnets, Phys. Rev. Lett. **122**, 247701 (2019).

[33] C. Xu, P. Chen, H. Tan, Y. Yang, H. Xiang, and L. Bellaiche, Electric-field switching of magnetic topological charge in type-I multiferroics, Phys. Rev. Lett. **125**, 037203 (2020).

[34] H. Fu and L. Bellaiche, First-principles determination of electromechanical responses of solids under finite electric fields, Phys. Rev. Lett. **91**, 057601 (2003).

[35] W. Kockelmann and U. Ruschewitz, Novel ternary alkali metal silver acetylides $MIAgC_2(MI = Li, Na, K, Rb, Cs)$, Angew. Chem. Int. Ed. **38**, 3492 (1999).

[36] J. Offermanns, U. Ruschewitz, and C. Kneip, Syntheses and crystal structures of novel ternary alkali metal gold acetylides $MIAuC_2(MI = Li, Na, K, Rb, Cs)$, Z. Anorg. Allg. Chem. **626**, 649 (2000).

[37] K. F. Garrity, High-throughput first principles search for new ferroelectrics, Phys. Rev. B **97**, 024115 (2018).

[38] T. E. Smidt, S. A. Mack, S. E. Reyes-Lillo, A. Jain, and J. B. Neaton, An automatically curated first-principles database of ferroelectrics, Sci. Data **7**, 72 (2020).

[39] X. Wang, Y. Ren, and M. Wu, Unconventional ferroelectricity with quantized polarizations in ionic conductors: High-throughput screening, J. Phys. Chem. Lett. **13**, 9552 (2022).

[40] M. Kruse, U. Petralanda, M. N. Gjerding, K. W. Jacobsen, K. S. Thygesen, and T. Olsen, Two-dimensional ferroelectrics from high throughput computational screening, npj Comput. Mater. **9**, 45 (2023).

[41] F. Ricci, S. E. Reyes-Lillo, S. A. Mack, and J. B. Neaton, Candidate ferroelectrics via *ab initio* high-throughput screening of polar materials, npj Comput. Mater. **10**, 15 (2024).

[42] X. Xu, T. Zhong, N. Zuo, Z. Li, D. Li, L. Pi, P. Chen, M. Wu, T. Zhai, and X. Zhou, High-T_C two-dimensional ferroelectric $CuCrS_2$ grown via chemical vapor deposition, ACS Nano **16**, 8141 (2022).

[43] P. Wang, Y. Zhao, R. Na, W. Dong, J. Duan, Y. Cheng, B. Xu, D. Kong, J. Liu, S. Du *et al.*, Chemical vapor deposition synthesis of intrinsic high-temperature ferroelectric 2D $CuCrSe_2$, Adv. Mater. **36**, 2400655 (2024).

[44] Z. Sun, Y. Su, A. Zhi, Z. Gao, X. Han, K. Wu, L. Bao, Y. Huang, Y. Shi, X. Bai *et al.*, Evidence for multiferroicity in single-layer $CuCrSe_2$, Nat. Commun. **15**, 4252 (2024).

[45] J. Xing, Y. Tang, J. Li, C. Wu, Y. Gu, X. Li, H. Zhang, M. Zhang, X. Wang, X. Zhou *et al.*, Intrinsic out-of-plane and in-plane ferroelectricity in 2D $AgCrS_2$ with high Curie temperature, Adv. Mater. **36**, 2407655 (2024).

[46] K.-J. Range, G. Engert, and A. Weiss, Darstellung und Kristallstruktur der Hochdruckphase AgAlS2-II/Preparation, and crystal structure of the high-pressure phase $AgAlS_2$-II, Z. Naturforsch. **29B**, 186 (1974).

[47] R. E. Cohen, Origin of ferroelectricity in perovskite oxides, Nature (London) **358**, 136 (1992).

[48] T. Murugesan and J. Gopalakrishnan, Rare earth copper sulphides ($LnCuS_2$), Indian J. Chem. **22A**, 469 (1983).

[49] J. Dismukes, R. Smith, and J. White, Physical properties and crystal structure of a new semiconducting I-III-VI_2 compound, $CuScS_2$, J. Phys. Chem. Solids **32**, 913 (1971).

[50] G. A. Jeffrey and M. Vlasse, Crystal structures of the red, yellow, and orange forms of mercuric iodide, Inorg. Chem. **6**, 396 (1967).

[51] D. Schwarzenbach, H. Birkedal, M. Hostettler, and P. Fischer, Neutron diffraction investigation of the temperature dependence of crystal structure and thermal motions of red HgI_2, Acta Crystallogr. Sect. B **63**, 828 (2007).

[52] W. Wang, S. Dai, X. Li, J. Yang, D. J. Srolovitz, and Q. Zheng, Measurement of the cleavage energy of graphite, Nat. Commun. **6**, 7853 (2015).

[53] T. Björkman, A. Gulans, A. V. Krasheninnikov, and R. M. Nieminen, van der Waals bonding in layered compounds from advanced density-functional first-principles calculations, Phys. Rev. Lett. **108**, 235502 (2012).

[54] H.-X. Deng, J.-W. Luo, S.-S. Li, and S.-H. Wei, Origin of the distinct diffusion behaviors of Cu and Ag in covalent

and ionic semiconductors, Phys. Rev. Lett. **117**, 165901 (2016).
[55] J. Peng, Y. Liu, H. Lv, Y. Li, Y. Lin, Y. Su, J. Wu, H. Liu, Y. Guo, Z. Zhuo *et al.*, Stoichiometric two-dimensional non–van der Waals $AgCrS_2$ with superionic behaviour at room temperature, Nat. Chem. **13**, 1235 (2021).
[56] B. Li, S. Li, H. Wang, L. Chen, L. Liu, X. Feng, Y. Li, J. Chen, X. Gong, and K.-W. Ang, An electronic synapse based on 2D Ferroelectric $CuInP_2S_6$, Adv. Electron. Mater. **6**, 2000760 (2020).
[57] B. Meyer and D. Vanderbilt, *Ab initio* study of ferroelectric domain walls in $PbTiO_3$, Phys. Rev. B **65**, 104111 (2002).
[58] P. Gao, J. Britson, J. R. Jokisaari, C. T. Nelson, S.-H. Baek, Y. Wang, C.-B. Eom, L.-Q. Chen, and X. Pan, Atomic-scale mechanisms of ferroelastic domain-wall-mediated ferroelectric switching, Nat. Commun. **4**, 2791 (2013).
[59] D. Meier and S. M. Selbach, Ferroelectric domain walls for nanotechnology, Nat. Rev. Mater. **7**, 157 (2022).
[60] J. Haeni, P. Irvin, W. Chang, R. Uecker, P. Reiche, Y. Li, S. Choudhury, W. Tian, M. Hawley, and B. Craigo, Room-temperature ferroelectricity in strained $SrTiO_3$, Nature (London) **430**, 758 (2004).
[61] A. Merchant, S. Batzner, S. S. Schoenholz, M. Aykol, G. Cheon, and E. D. Cubuk, Scaling deep learning for materials discovery, Nature (London) **624**, 80 (2023).

End Matter

Interplay between FQFE and other ferroic orders—As FQFE follows different symmetry principles than conventional ferroelectricity, FQFE systems with centrosymmetry usually lack piezoelectricity and pyroelectricity. However, FQFE can coexist with properties like piezoelectricity, ferroelasticity, and multiferroicity, allowing it to respond to multiple external stimuli in addition to electric fields. Note that the presence of a nonzero polarization difference between two equivalent FQFE states becomes more intuitive when considering finite systems (see Sec. 10 of SM [18]). However, we emphasize that FQFE is a bulk phenomenon as the magnitude of polarization difference between two equivalent FQFE states remain unaffected by the presence of boundaries.

Switchability of FQFE and broader range of FQFE candidates—Note that though we did not compute switching barriers for all the FQFE candidates in Tables S1 and S2 [18], there is still a large possibility of experimental realization FQFE in those systems. This is because the barriers can decrease dramatically in the presence of domain walls, strains, defects, etc. [57–60]. For example, for the traditional ferroelectric $PbTiO_3$, the existence of 90° and 180° domain wall can lead to a minuscule barrier for reversal of polarization [57]. In addition, there is a significant number of materials predicted by DFT in the database that are expected to become candidates for FQFE. Using our proposed symmetry strategy, we identified 2759 materials predicted by DFT that have robust stability and exhibit FQFE properties. Among them, there are 411, 1062, and 1286 materials from Materials Project [19], C2DB [20,21], and GNoME database [61], respectively.